Low concentration *E. coli O157:H7* bacteria sensing using microfluidic MEMS biosensor

Cite as: Rev. Sci. Instrum. **89**, 125009 (2018); https://doi.org/10.1063/1.5043424
Submitted: 08 June 2018 . Accepted: 03 December 2018 . Published Online: 28 December 2018

Shibajyoti Ghosh Dastider, Amjed Abdullah, Ibrahem Jasim, Nuh S. Yuksek, Majed Dweik, and Mahmoud Almasri

Low concentration *E. coli O157:H7* bacteria sensing using microfluidic MEMS biosensor

Shibajyoti Ghosh Dastider,[1] Amjed Abdullah,[1] Ibrahem Jasim,[1] Nuh S. Yuksek,[1] Majed Dweik,[2] and Mahmoud Almasri[1,a)]
[1]*Department of Electrical and Computer Engineering, University of Missouri, Columbia, Missouri 65211, USA*
[2]*Department of Co-operative Research, Lincoln University, Jefferson City, Missouri 65101, USA*

(Received 8 June 2018; accepted 3 December 2018; published online 28 December 2018)

This paper reports the design, fabrication, and testing of a microfluidic MEMS biosensor for rapid sensing of low concentration *Escherichia coli* O157:H7. It consists of a specially designed focusing and sensing region, which enables the biosensor to detect low concentration of bacterial cells. The focusing region consists of a ramped vertical electrode pair made of electroplated gold along with tilted thin film finger pairs (45°) embedded inside a microchannel. The focusing region generates positive dielectrophoresis force, which moves the cells towards the edges of the tilted thin film electrode fingers, located at the center of the microchannel. The fluidic drag force then carries the focused cells to the sensing region, where three interdigitated electrode arrays (IDEAs) with 30, 20, and 10 pairs, respectively, are embedded inside the microchannel. This technique resulted in highly concentrated samples in the sensing region. The sensing IDEAs are functionalized with the anti-*E. coli* antibody for specific sensing of *E. coli* 0157:H7. As *E. coli* binds to the antibody, it results in an impedance change, which is measured across a wide frequency range of 100 Hz–10 MHz. The biosensor was fabricated on a glass substrate using the SU8 epoxy resist to form the microchannel, gold electroplating to form the vertical focusing electrode pair, a thin gold film to form the sensing electrode, the finger electrodes, traces and bonding pads, and polydimethylsiloxane to seal the device. The microfluidic impedance biosensor was tested with various low concentration bacterial samples and was able to detect bacterial concentration, as low as 39 CFU/ml with a total sensing time of 2 h. *Published by AIP Publishing.*
https://doi.org/10.1063/1.5043424

I. INTRODUCTION

Foodborne pathogens cause illnesses in approximately 48 × 10^6 people every year, resulting in 128 000 hospitalizations and 3000 fatalities.[1] The Centers for Disease Control and Prevention (CDC) indicates that in 2014 between 20 and 40 potential food poisoning or related clusters was monitored each week and more than 220 multistate clusters were investigated. This resulted in the identification of 68 confirmed or suspected vehicles of transmission and then recalled a variety of foods including sprouted chia powder, caramel apples, ground beef, and clover sprouts.[2] A foodborne outbreak is the result of transmission of pathogens to humans via consumption of contaminated food and drink. CDC reports that more than 250 pathogens and toxins are known to cause foodborne illnesses. Nearly all of them can cause an outbreak. Among them, various strains of *Escherichia coli*, *Salmonella*, and *Listeria monocytogenes* are primarily responsible for many outbreaks.[3] The economic burden of health losses due to foodborne outbreaks is enormous. Foodborne outbreaks have the potential to cause massive economic devastation due to medical costs and product recalls. In the Unites States, the annual cost of foodborne illnesses was estimated to be $\$77.7 \times 10^9$.[4] Hence, developing foodborne pathogen prevention and sensing techniques is very important. *E. coli* O157:H7 one of the most harmful foodborne pathogenic strains in North America produces the Shiga toxin that damages the intestine lining and causes anemia, stomach cramps, and bloody diarrhea. Sometimes, it causes serious complications including hemolytic uremic syndrome (HUS) and thrombotic thrombocytopenic purpura (TTP).[5–7]

Although the official food screening procedure established by the Food and Drug Administration (FDA) to identify pathogenic bacteria in food is very reliable, they require 5-7 days and therefore are not suitable for real time monitoring of possible outbreaks. By the time the bacteria are detected, the contaminated product may already be sold and consumed. There are several sensing methods for *E. coli* O157:H7, such as traditional culture methods, immuno-assays, and molecular methods. Some of these methods have high sensitivity and reliability, but their application in food safety is limited due to time-constraint.[8] Conventional sensing methods, including cell culture, enzyme-linked immunosorbent assay (ELISA), and polymerase chain reaction (PCR) based tests, are generally labor-intensive.[9,10] Loop mediated isothermal amplification (LAMP) integrated with acoustic detection was used for *Salmonella* detection in milk products. 3 h of pre-enrichment was performed, followed by immuno-magnetic bead cell capturing. Then, DNA amplification was performed using the LAMP method. The detection limit was 2 or 3 CFU/μl.[11] In recent years, studies on biosensing methods have increased significantly and become one of the most active research areas for pathogen sensing. Electrochemical biosensors are widely recognized as powerful analytical tools due to their

a)Author to whom correspondence should be addressed: almasrim@missouri.edu. Tel.: +15738820813.

low manufacturing cost, shorter analysis and response time, and portability. A single walled carbon nanotube (SWCNT) electrochemical immunosensor was implemented as antibody bio-conjugates for the label-free detection of *Staphylococcus aureus*. Anti-*S. aureus* antibodies were bonded to the SWCNTs and then immobilized on the electrodes which results in change in current flow. The limit of detection was from 10 to 10^7 CFU/ml.[12] A quartz crystal microbalance nanoplatform for the rapid, sensitive, and label-free detection of *E. coli* was used. Under optimal conditions, the frequency of the quartz crystal microbalance biosensor was directly proportional to the concentration of the antigen with a dynamic range from 0.5 mg ml^{-1} to 5 ng ml^{-1}, a minimum detection limit of 5 ng ml^{-1}, and a sensitivity of 0.037 Hz g ml^{-1} cm^{-1}.[13] Moreover, a new approach for the detection of *Salmonella enteritidis* that coupled with an SPR immunosensor and Fe_3O_4 MNP separation was described where *S. enteritidis*-immunoMNPs conjugates were directly flowed over the sensor surface modified with an anti-*Salmonella* polyclonal antibody (PAb) and a detection of 14 CFU/ml with a good linear signal range at 1.4×10^1–1.4×10^9 CFU/ml.[14] A development of a thermally reduced graphene oxide (rGO)-based FET platform modified with *E. coli* antibodies (anti-*E. coli*) was achieved for the detection of single *E. coli* bacteria.[15] Some other group developed a sample processing approach for real-time PCR-based detection of *Salmonella* from raw chicken breast through the combination of targeted cell capture by the ion-mobility spectrometer (IMS) and highly efficient amplification of genomic DNA by multidimensional analysis (MDA) and approached a detection limit of 10 CFU/ml.[16] Several microfluidic-based sensing methods have been utilized for bacterial sensing, which includes particle counters, biosensors, and on-chip microbial culture-based methods. Impedance biosensors are one of the most promising sensing technologies, among various label-free sensing platforms, due to simplicity and adaptability with relevant lab-on-a-chip applications.[17] The Surface Plasmon Resonance (SPR) technique was used for the detection of *E. coli* O157:H7 and *Salmonella* in hamburger and cucumber samples. It uses gold nanoparticles and a biotinylated secondary antibody for the detection of *E. coli* O157:H7 and *Salmonella*. The method incorporates the use of both poly-(carboxybetaine acrylamide) (pCBAA) and SPR. The detection limit of the device is 17 CFU/ml for *E. coli* and 7000 CFU/ml for *Salmonella* with a total testing time of 80 min.[18] In some early electrochemical impedance biosensors, large metal rods or wires were used as electrodes to measure impedance.[19,20] To improve the sensitivity and miniaturize the size of the sensor system, the potential of microelectrode-based sensor systems was considered and combined with the traditional sensing system. Among microelectrodes, interdigitated microelectrode arrays (IDMAs) are most popular. IDMA has some considerable advantages over other types of electrode systems. It has low ohmic drop, fast establishment of steady-state, and also rapid reaction kinetics.[21,22] The increased signal-to-noise ratio and the low response time also enable rapid sensing.[23] Moreover, IDMA has a significant advantage over three or four electrode systems as this sensing system does not require a reference electrode and it provides simple means to obtain steady-state response.[24,25] Interdigitated microelectrodes can produce maximum change in impedance, help reduce the sensing time, and work in a two-electrode system,[26–28] hence simplifying the fabrication and improving performance of electrochemical biosensors.[29–31] Disposable screen printed impedance biosensors based on different types of electrodes have recently been reported, which offers cost-effective sensing methods.[32,33] In recent years, dielectrophoresis (DEP) has been incorporated to improve the sensing capability of the electrochemical sensing systems and lab-on-a-chip devices.[34–36] DEP is used to separate several types of cells from each other,[37] to isolate bacterial cells,[38,39] and in the filtration of bacterial cells from similar sized particles.[40]

In this paper, we present an easy to fabricate microfluidic MEMS biosensor for rapid and specific detection of *Escherichia-coli* O157:H7. This biosensor consists of a focusing and sensing region and is capable of detecting bacterial concentration as low as 39 CFU/ml. The focusing region electrodes focus the bacteria towards the center-line of the channel using positive dielectrophoretic (*p*-DEP) force, while fluidic drag force directs the bacteria towards the sensing region. The sensing region electrodes were functionalized with the *E. coli* specific antibody to immobilize the bacteria for impedimetric sensing. The change in impedance due to antigen-antibody binding is detected using an impedance analyzer. The biosensor achieves high selectivity using the *E. coli* 0157:H7 specific antibody as the bio-recognition element. The overall sensing time is under 2 h, as it requires no enrichment steps and minimal sample processing.

II. MATERIALS AND METHODS

A. Biosensor design

The microfluidic MEMS biosensor consists of two specially designed functional regions, called the focusing region and the sensing region. A 3D schematic view of the biosensor is shown in Fig. 1. The focusing region consists of a focusing electrode pair, embedded inside a ramped microfluidic channel. The starting and end widths of the microfluidic channel in the focusing region are 300 μm and 100 μm, respectively. The focusing electrode consists of vertical side walls along with tilted (45°) thin film finger electrodes. This focusing electrode pair generates a non-uniform electrode field, which exerts *p*-DEP force to drive and focus the bacterial cell towards the center of the microfluidic channel. Towards the end of the focusing region, the 100 μm wide microfluidic channel is split into three equal width (33 μm) sub-channels, each of which carry out specific functions. The focused cells flow in a streamed line fashion through the center sub-channel towards the sensing region. The outer two sub-channels carry bulk fluid to the waste outlets. This sensing region consists of three sets of interdigitated microelectrode arrays (IDEAs), each with a varying number of fingers (30, 20, and 10 pairs). Each array has dedicated bonding pads. These IDMAs allow detection of very low bacterial concentration, improving the sensitivity of the biosensor. For all three IDMA arrays, electrode finger's length, width, and spacing were 20 μm, 10 μm, and 10 μm, respectively. Each electrode array has a separate pair of bonding pads to interface the biosensor with external sources and

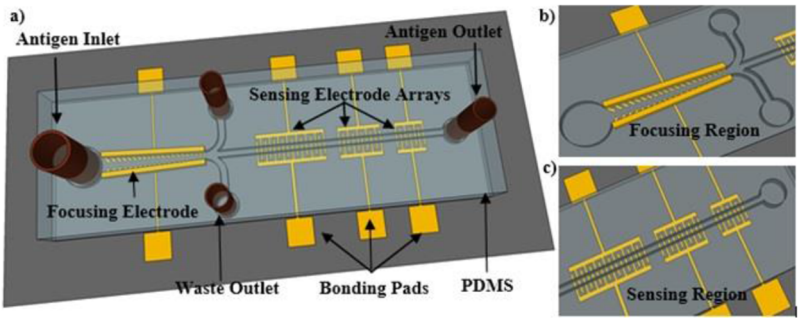

FIG. 1. Schematic of (a) the microfluidics biosensor for *E. coli* O157:H7 sensing with PDMS top cover and fluidic connectors, (b) magnified view of the focusing region, and (c) sensing region electrode arrays embedded under the SU-8 microchannel.

data acquisition systems, such as a function generator and an impedance analyzer. The microfluidic channel was fabricated on top of the electrode arrays and is embedded in a permanent SU-8 photoresist layer. The depth of the microchannel is 15 μm throughout its length and is defined by the SU-8 resist thickness. The microchannel has a total of four inlet-outlet fluidic ports. A pre-cured thick polydimethylsiloxane (PDMS) block with an inlet-outlet opening is used to seal-off the microchannel. A second thicker PDMS slab with a fluidic connector is used to interface the microchannel with external fluidic tubing. The sealed biosensor is then wire-bonded to a printed circuit board.

B. Microfabrication

The microfluidic biosensor was fabricated on a glass substrate which was initially cut to smaller sizes to fit only a single device. The substrate was first wet cleaned with Piranha solution for 5 min to remove any contaminants from the surface. The process flow of the biosensor consists of series of photolithography and surface micromachining and is shown in Fig. 2. (1) A 4 μm thick layer of the negative resist, SU-8 2005, was spin coated on the substrate and subjected to UV flood exposure.

After post exposure bake, the substrate was hard baked at 150 °C for 30 min to completely cure and cross-link the SU-8 2005 layer. This SU-8 2005 layer serves an important purpose of adhering the subsequent top SU-8 2025 microchannel layer to the glass substrate and prevents the peeling effect during operation. (2) A magnetron RF sputtering was utilized to deposit 50 nm Titanium (Ti) and 150 nm gold (Au) thin films at 4 mTorr. The Ti thin film acts as an adhesion layer to improve the adhesion of the Au thin film to the underlying SU-8 2005 layer. The Au thin films serve as the seed layer for Au electroplating to create the vertical sidewall electrodes. The Au layer was patterned and wet etched using a mixture of potassium iodide (KI) and iodine (I2) to create the tilted (45°) thin film finger pairs in the focusing region, interdigitated electrode (IDE) arrays in the sensing region, trace-lines, and bonding pads.

From left to right, the three sensing electrode arrays consist of 30, 20, and 10 pairs of interdigitated electrodes. Each electrode's fingers are 100 μm in length, 10 μm in width, and 10 μm apart from each other. All IDE arrays have a pair of bonding pads for electrical connections. An optical image of the patterned electrodes is shown in Fig. 3. (3) A photoresist mold (AZ4620) was formed, and Au with a thickness of 15 μm was electroplated to create the focusing electrodes. (4) The photoresist was washed away, and the Ti layer was etched using diluted hydrofluoric acid (HF). (5) The microchannel was defined using SU-8 with a thickness of 25 μm. The SU-8 microchannel was then treated to improve the biocompatibility by exposing it at 450 mJ/cm^2 UV flood for 1 h followed by 150 °C oven baking for 24 h. The microchannel is then exposed to oxygen plasma for 20 s and washed with isopropanol (IPA) for 1 min. (6) The PDMS slabs were made to serve as the top cover along with fluidic connectors. Scanning Electron Microscope (SEM) micrographs of the microfluidic MEMS biosensor before sealing the channel are shown in Fig. 4. (7) An oxygen plasma treatment was applied on the PDMS cover in order to change its surface to hydrophilic, and then, SU-8 was spin coated onto it to serve as glue. The oxygen plasma step was used to improve the adhesion of SU-8 to PDMS. (8) The PDMS was aligned with the microchannel and bonded under pressure at 48 °C on a hotplate plate for 1 h. The PDMS/SU-8 cover and SU-8 microchannel cross-linked and formed a strong bond. During the bonding process, it was found that lower bonding temperature would cause weak bonding and air

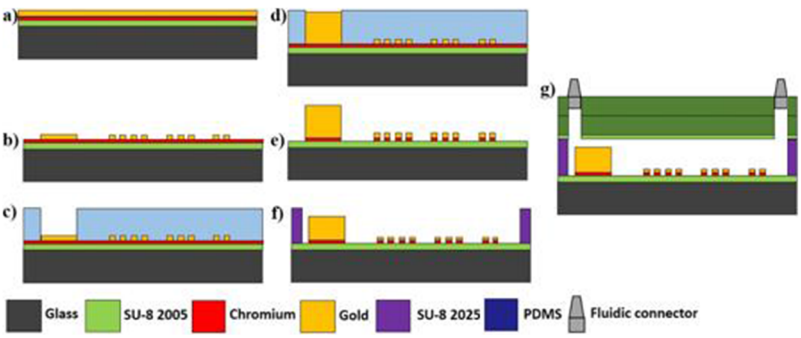

FIG. 2. Cross-sectional view of the process flow of the microfluidic biosensor. (a) Cr/Au is sputtered on a SU-8 2005 coated glass substrate, (b) Au is patterned on a SU-8 2005 to create the interdigitated electrode arrays, traces, bonding pads, and seed layer for electroplating the focusing electrode, (c) photoresist mold is patterned for Au electroplating, (d) Au is electroplated to create a vertical side wall electrode for the focusing region, (e) photoresist mold is removed, and Cr is etched, (f) SU-8 2025 is spin-coated and patterned to create a microfluidic channel, and (g) a PDMS cover with inlet-outlet holes is cured and bonded to the microchannel layer using the O_2 plasma technique.

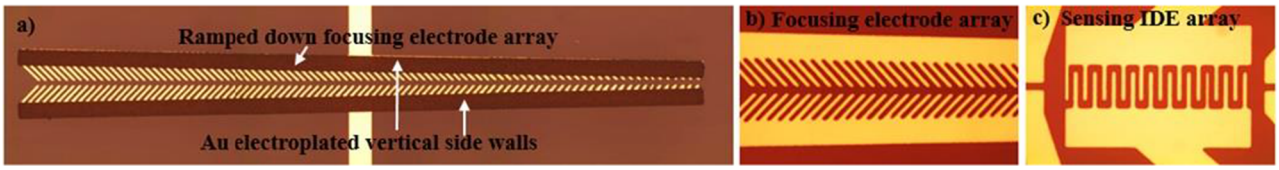

FIG. 3. Optical images of (a) the entire focusing region with a ramped down focusing electrode array, (b) magnified view of the tilted focusing electrode fingers, and (c) magnified view of the sensing electrode array.

bubbles were trapped in the interface, and the higher bonding temperature would cause SU-8 to flow into the microchannel and block it. The optimized bonding temperature was between 45 and 50 °C. This was followed by UV flood exposure (450 mJ/cm^2) and hard baking at 120 °C or 20 min in order to fully cure the SU-8 layer. (9) The device was attached, and wire was bonded to a printed circuit board.

C. Bacterial sample preparation and enumeration

The bacteria used in this study, *E. coli* O157:H7 (ATCC 700728), were obtained from American Type Culture Collection (ATCC), USA. *E. coli* (EC) broth (Fluka Analytical, USA) was used for culturing *E. coli* O157:H7. To prepare the sample, a loop full of stock culture was inoculated into the EC broth containing tubes. Inoculated tubes were incubated at 37 °C for 18 h. After incubation, the 18 h culture measuring 1 ml was centrifuged (Horizon 642VES, Drucker Company, PA) at 3200 rpm for 10 min. After the centrifugation, the cell pellet was obtained by removing the supernatant, and the cells were re-dispersed in 1 ml of deionized (DI) water to wash the cell pellet. The re-dispersed cells were centrifuged again, and the step was repeated. The prepared 1 ml *E. coli* O157:H7 cells in DI water were subjected to serial dilution to get a low cell number for the test. For serial dilutions, 1 ml of the sample was taken and mixed well with a tube containing sterile 9 ml of DI water (dilution 1). From dilution 1, 1 ml of the content was taken and mixed with another tube containing 9 ml of sterile deionized water (dilution 2). Subsequent dilutions were prepared similarly. 1 ml of lowest dilutions that give desired probable concentration of bacteria was taken for the sensing process. Another 1 ml of the same sample was subjected to Colony Forming Unit (CFU) analysis to get the bacterial concentration in the sample, where 1 ml of the sample was inoculated on Tryptic Soy Agar (Fluka Analytical, USA) plates and incubated for 24 h at 37 °C. After incubation, the plates were observed for a number of CFUs present.

D. Antibody immobilization and antigen capturing

The goat anti-*E. coli* O157:H7 polyclonal antibody (Ab) (Meridian Life Sciences, USA) was injected into the microchannel [at the concentration of 10 μg ml^{-1} in deionized (DI) water] through the outlet, and the pump was stopped before the solution reached the fluidic junction. The anti-*E. coli* antibody non-specifically gets absorbed to the sensing electrode surface. The antibody solution was kept in the microchannel for at least 30 min to achieve highest surface coverage, minimizing any subsequent nonspecific adsorption. After 30 min, the liquid was then pumped out, and any unbound antibodies were washed away using DI water. Next, the prepared *E. coli* O157:H7 cells were pumped into the microchannel through the inlet, and once the microchannel was filled, the flow was stopped for 30 min to allow the antigens to bind to the antibody. This immuno-complex (antigen-antibody binding) on the surface of the electrode resulted in a change of measured impedance.

E. Experimental setup

The antibody, antigens, and other fluidics used in the experiment were injected at various volumetric flow rates using a syringe pump (a Harvard Apparatus PHD 2000). An inverted microscope with a CCD camera was used to capture optical images of the biosensor during the experiment. The impedance across the sensing electrode array was measured using an Agilent 4294A impedance analyzer. The impedance was measured by applying an AC voltage of 0.5 V (peak-to-peak voltage) across the sensing electrode array. The corresponding

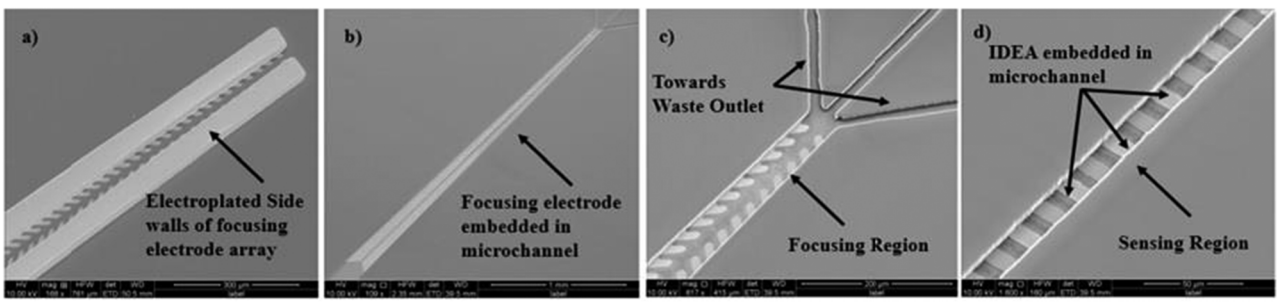

FIG. 4. SEM micrographs of (a) electroplated focusing electrodes, (b) focusing electrodes embedded in the microchannel, (c) focusing electrodes with the microchannel branches, and (d) one of the sensing electrode arrays embedded under the SU-8 microchannel.

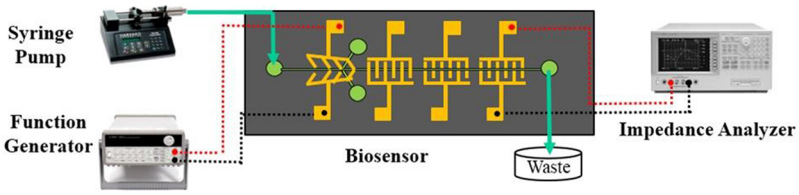

FIG. 5. An optical image of the experimental setup. The biosensor was placed on an inverted microscope with its inlets and outlets connected to a syringe pump and reservoirs, respectively. Electrical connections were made to the impedance analyzer and the computer for data acquisition. The function generator was used to deliver the required AC signal for DEP.

impedance values were measured for frequencies between 100 Hz and 10 MHz. A function generator was used to apply AC voltage at various frequencies at the focusing IDE array in order to generate *p*-DEP and optimize the focusing capability of the device. The experimental setup for characterizing the fabricated impedance biosensor is shown in Fig. 5.

III. RESULTS AND DISCUSSION

A. Modeling and simulation

The modeling was performed using COMSOL Multiphysics 4.2 and LISA 8.0 software. Figure 6(a) shows the electric field (E-field) distribution across the length of the focusing region for a 5 V AC signal. Analysis shows the presence of high E-field at the center of the ramped microchannel, while lower E-field, as we move away from the center. As cells flow through the focusing region, they are subjected to non-uniform E-field. This non-uniform E-field exerts dielectrophoretic forces on the cells, which enable them to move towards the center of the ramped microchannel.

Although the tilted thin film finger pairs dominate the focusing process, the thick electroplated sidewall electrodes assist the *p*-DEP process by extruding the E-field along the Z axis, as shown in Fig. 6(b). This enables a uniformly distributed DEP force throughout the channel height. In addition, the ramp down feature of the channel generates hydrodynamic forces that aided the focusing process. In conclusion, this design will enable concentrating the pathogenic samples significantly and thus increase its lower sensing limit. The bulk fluid, which is free of pathogens, will keep flowing toward the outer channel into the waste outlets. The sensing of *E. coli* will be based on impedance measurements using an IDE array. The sensing regions consist of a series of 3 interdigitated electrode (IDE) arrays each with a varying number of fingers (30, 20, and 10 pairs). The IDE arrays are connected to an impedance analyzer to measure the change in impedance. As impedance is measured, the impedance analyzer applies an AC signal to the IDE. This will generate a varying E-field across the height of the channel. The goal is to reduce the electric field strength, in order to reduce the effect on the cell in terms of stress and survivability.

The E-field distribution across the height of the microchannel on top of the interdigitated electrodes was simulated using COMSOL Multiphysics, as shown in Fig. 6(c). The finger's overlap length, width, and spacing were 15 μm, 10 μm, and 10 μm, respectively. The modeling results show that at 500 mV, the electric field strength is minimum across the height of the channel and maximum in vicinity to the electrode surface. This 500 mV AC signal at varying frequencies (100 Hz–10 MHz) was applied in the sensing region impedance measurement. The impedance of each IDE array along the channel will be measured separately before and after antibody-antigen binding using an impedance analyzer connected to an electrical switching circuit. This will ensure capturing and sensing of a single cell or several cells by one or more IDE arrays along the channel.

B. Cell focusing

Biosensor's precision and sensitivity can be improved by driving cells or micro particles into a small, spatially well-defined volume within the microchannel. In our design, driving cells into the center of the microchannel are significant because it prevents the microchannel from clogging and also improves the sensitivity of the measurement, by increasing the concentration of the bacterial cell. Dielectrophoresis (DEP) is used to manipulate the location of the cells inside the microchannel and can be defined as the translational motion of a dielectric particle or cell in a suspending medium under the influence of

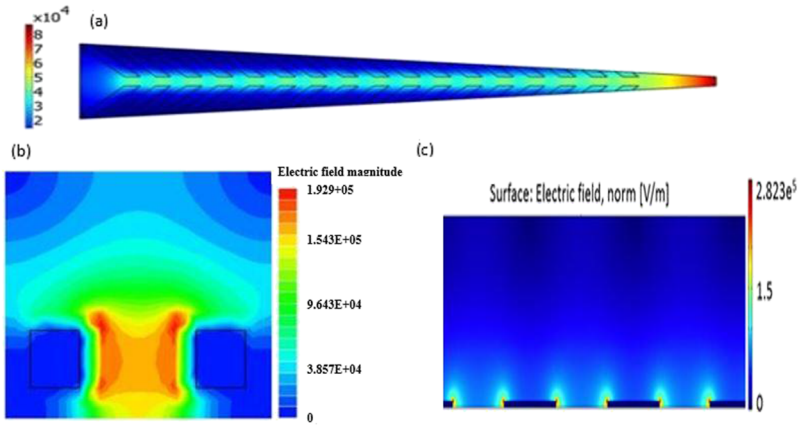

FIG. 6. The simulation of the E-field across (a) the length of the focusing region, (b) the height of the channel in the focusing region, and (c) the sensing IDE array at 500 mV is shown.

a non-uniform AC E-field.[41] This non-uniform E-field induces a net force in a dielectric particle or cell directed either to a region of maximum or minimum E-field strength. The driving force direction is determined by the following two factors: permittivity of the particle compared with that of the medium surrounding the particle and the frequency of the applied E-field

$$F_{DEP} = 2\pi\varepsilon_m r^3 \cdot [\mathrm{Re}|F_{CM}(\omega)|]\nabla\left|\vec{E}\right|^2, \quad (1)$$

where $\nabla\left|\vec{E}\right|^2$ is proportional to the gradient and strength of the applied electric field. Re|FCM(ω)| is referred to as the Clausius Mossotti (C-M) factor. It determines the effective polarizability of the particle and is expressed by the following equation:

$$\mathrm{Re}|F_{CM}(\omega)| = \frac{\varepsilon_p - \varepsilon_m}{\varepsilon_p + 2\varepsilon_m} + \frac{3(\varepsilon_m\sigma_p - \varepsilon_p\sigma_m)}{\tau_{MW}(\sigma_p + 2\sigma_m)^2(1 + \omega^2\tau_{MW}^2)}, \quad (2)$$

where ε_m, σ_m and ε_p, σ_p are the absolutely permittivity and conductivity of the media and the spherical particle, respectively. The direction of DEP force is determined by the sign of the C-M factor which in turn is a function of the frequency of applied E-field. For positive DEP (*p*-DEP), the C-M is positive, and the particle is attracted to an electrical field maximum, whereas for negative DEP (n-DEP), the particle moves towards the electrical field minimum. Movement of particles inside a microchannel can be controlled in various ways, such as by changing the electrode design, varying the electrical signal, and modifying the liquid media properties, where the particles which are suspended refer to the Maxwell-Wagner charge relaxation time and are expressed as follows:

$$\tau_{MW} = \frac{\varepsilon_p + \varepsilon_m}{\sigma_p + 2\sigma_m}. \quad (3)$$

In this biosensor, we used a ramped down focusing region to pre-concentrate *E. coli* cells. The phenomenon of *p*-DEP was employed to focus and direct the cells towards a centre channel which has a diameter as small as one-third of the first channel. Thus, cell concentration will increase significantly in the sensing channel.

When bacteria flow through the channel in addition to *p*-DEP force, they are also subjected to a frictional hydrodynamic force ($\vec{F}_{drag}$). This can be defined by the following equation, where $\vec{v}$ is the relative velocity between the cell and the flow, η is the fluid viscosity, and *r* is the cell radius:

$$\vec{F}_{drag} \approx \eta r\vec{v}. \quad (4)$$

The ratio of the drag force to the velocity $\frac{\vec{F}_{drag}}{\vec{v}} = k_{drag}$ is called the drag coefficient and is roughly equivalent to the product of viscosity and longest dimension of the cell. Under *p*-DEP, the cells get attracted towards the highest electric field and move the bacterial cells towards the centre of the microchannel. To flow the cells to the sensing region, a minimum flow is required. At equilibrium, the hydrodynamic and DEP forces are equal, which gives us the minimum velocity required to move the cells towards the sensing region in a controlled fashion

$$\vec{v}_{min} < \frac{\varepsilon_m r^2}{3\eta} Re[K]\frac{\partial E^2}{\partial x}\vec{v}. \quad (5)$$

Hydrodynamic drag force in conjunction with the *p*-DEP force creates a streamlined cell flow, through the centre of the narrow channel towards the sensing electrode array, which prevents clogging of the microchannel.

The focusing effect of the biosensor was tested and demonstrated using polystyrene microbeads with a diameter of 5 μm to study the focusing capability of the device. An AC signal of 5 Vp-p, 5 MHz was applied at the focusing electrode to generate a non-uniform electrical field across the width of the microchannel. A design of experiment (DOE) was performed to experimentally determine the optimal amplitude and frequency. The polystyrene microbeads suspended in DI water were injected into the microchannel with a flow rate of 2-4 μl/min and those with the help of dielectrophoresis were focused towards the centre of the microchannel, as shown in Fig. 7. To demonstrate the device focusing effect, microbeads were used to replace *Salmonella* cells. The focusing effect mostly depends on the relative permittivity of the dielectric object. *Salmonella* and the used polystyrene microbeads have a convergent relative permittivity of 4.5-6.5[42,43] and 4,[44] respectively. Although there is a small difference between microbeads and *E. coli* in relative permittivity, it has only a small effect on the optimum value of the applied AC frequency. The frequency of the applied AC is an important factor in defining the focusing effect of the microbeads and the cells since the used solution in both experiments is the same.

C. Impedance measurement and analysis

Initially, the impedance response of each sensing electrode array was measured over a frequency range of 100 Hz–10 MHz by filling the channel with DI water. The bare electrode array's impedance value was used to confirm the adsorption of the antibody on the gold electrode surface. The anti-*E. coli* IgG antibodies (Abs) were injected into the sensing electrode microchannel via the antibody inlets and were non-specifically adsorbed on the electrode surface to ensure selective sensing of *E. coli* cells. As the antibodies were adsorbed, the impedance of the electrode array changed.

This change of impedance demonstrates that the antibodies are successfully adsorbed on the electrode surface. The

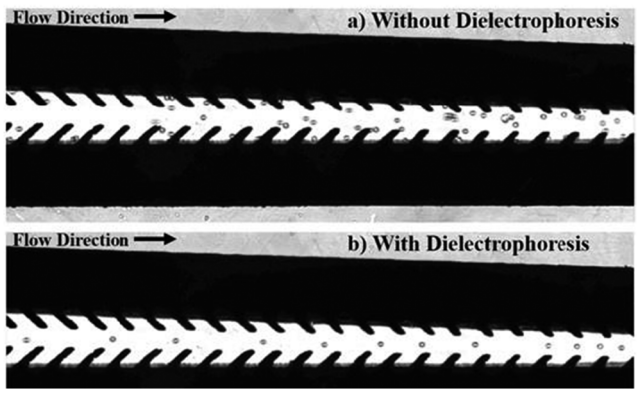

FIG. 7. Optical images of the focusing electrode region, showing microbeads flowing (a) randomly without *p*-DEP and (b) in a controlled streamlined fashion under influence of *p*-DEP.

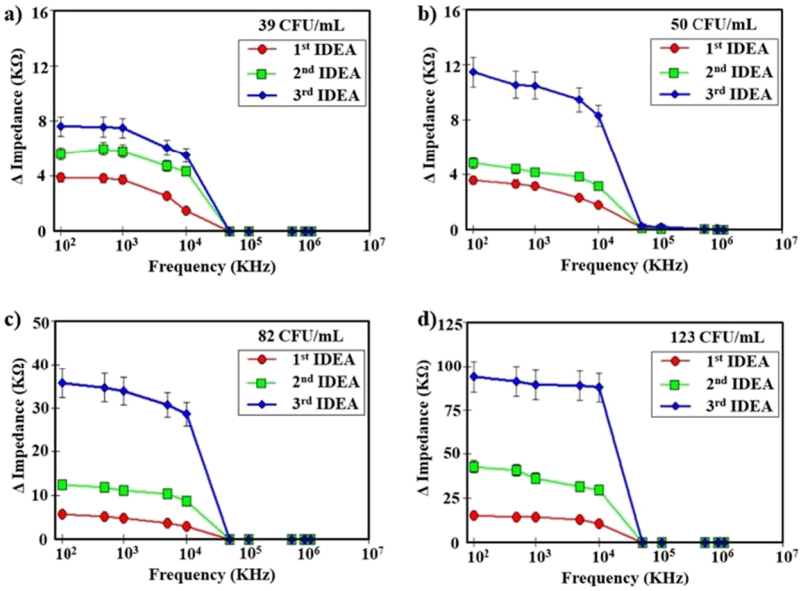

FIG. 8. Impedance response of all three-sensing arrays measured independent of each other: (a) 39 CFU/ml, (b) 50 CFU/ml, (c) 82 CFU/ml, and (d) 123 CFU/ml for a frequency range of 100 Hz–10 MHz.

measured electrode-antibody impedance was used as the baseline impedance in order to accurately determine the *E. coli* impedance. As the *E. coli* samples were pumped and filled the microchannel, the flow was stopped, and the solution was left on top of the sensing electrodes for 30 min to successfully bind to the antibodies, which was determined to be sufficient for efficient binding.[21] The antigen-antibody binding resulted in a change in the total measured impedance. The *E. coli* impedance was calculated by subtracting the measured baseline impedance from the total measured impedance. It was then correlated to the actual concentration of the *E. coli* testing samples that were obtained from a traditional cell plating method. Several low concentrations of *E. coli* samples were tested. Before impedance measurement can be performed, the surface of the sensing IDEAs was functionalized using the anti-*E. coli* antibody. As the targeted pathogen, *E. coli*, reaches the sensing electrodes and it comes in contact with the antibody on the IDEA surface. This results in Ab-Ag binding on the IDEA surface and leads to a change in impedance, which is measured using an impedance analyzer. The impedance analyzer records over a frequency range of 100 Hz–1 MHz. Figure 8 shows the impedance response of the biosensor for various low concentrations of *E. coli* test samples. The equivalent circuit analysis indicates that, at higher frequencies, the impedance response is negligible.

At higher frequencies (>50 kHz), the impedance response becomes independent of the bacterial concentration immobilized on the sensor surface. This can be explained using the equivalent circuit. As frequency is increased, the stray capacitance dominates the impedance and the effect of double layer capacitance (Cdl) is minimized. As a result, contribution of bacterial impedance reduces, and the response becomes dependent on the dielectric properties of the system and the resistance of the test solution. At lower frequencies, the impedance responses are largely dominated by the bacterial presence and can be clearly distinguished from one concentration to another. The lower concentration samples have a limited number of cells to bind to the sensor surface, while larger concentrations have many cells available to bind to the antibody on the sensor surface. As the available surface area was shirked due to *E. coli* binding, the double layer capacitance decreased. This phenomenon is believed to be responsible for overall increases in impedance. From the analysis of the obtained response, we see that the impedance response increases with bacterial concentration. Thus, it can be inferred that the response is dependent on both frequency and bacterial concentration. The impedance response was measured for each individual sensing array. The Bode plot of the impedance response demonstrates that the 3rd (smallest, 10 pairs of interdigitated electrodes) sensing array recorded the highest change in impedance. This demonstrated the fact that the change in impedance is dependent on the available surface area post Ab-Ag binding. This proposed biosensor was able to detect *E. coli* O157:H7 concentration as low as 39 CFU/ml with a

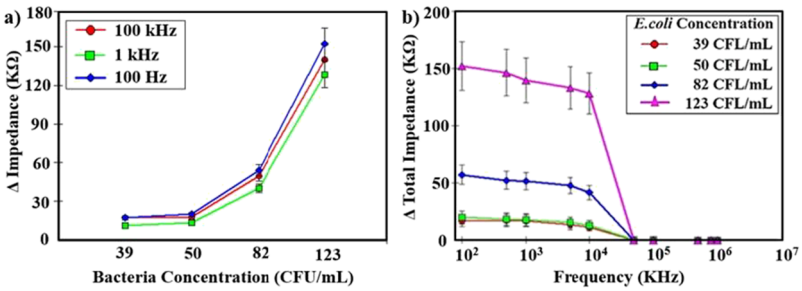

FIG. 9. Comparison of (a) impedance response of various concentrations at 100 Hz, 1 kHz, and 100 kHz frequency and (b) combined total impedance response of the biosensor for various concentrations of *E. coli* 157:H7 for a frequency range of 100 Hz–10 MHz.

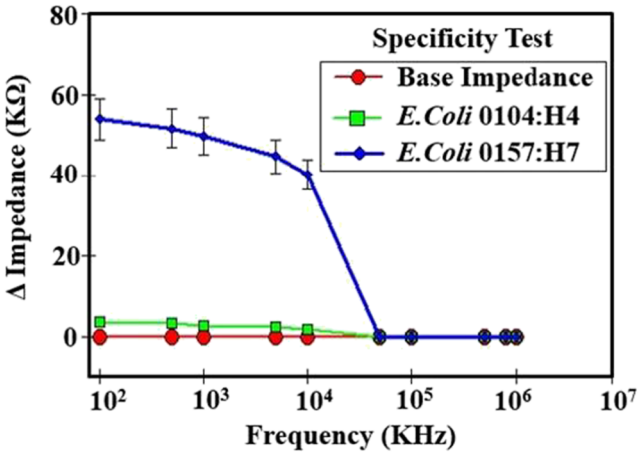

FIG. 10. Impedance response obtained from specificity testing with an antigen which does not bind to anti-*E. coli*.

rapid turnaround time of 2 h. This also indicated a greater than threefold improvement in the lower sensing capability of the biosensor, compared to our previous design. Figure 9 shows a comparison of the total combined impedance response of all three-sensing arrays. The impedance response shows that for higher concentration, samples produce an overall larger change in measured impedance. This indicated that the change in impedance is a strong function of the cell concentration.

D. Specificity of the biosensor

The biosensor was tested with different serotypes of *E. coli* O104:H4 cells in order to confirm its specificity. The measured response was plotted in Fig. 10. The plot shows no significant difference in the impedance value with respect to the base impedance of the IDE array. This was expected as the sensing electrode surface was modified specifically using the anti-*E. coli* O157:H7 antibody. Although some *E. coli* O104:H4 cells may have non-specifically been bound to the electrode surface, their numbers were so insignificant that it did not produce enough change in the impedance value. This also suggested that good antibody coverage of the electrode's surface was obtained and the anti-*E. coli* antibody did not attach to the non-*E. coli* O157:H7 cells. This demonstrated the specificity of the impedance biosensor in the presence of non-target bacterial cells.

IV. CONCLUSION

In this study, we established a microfluidic MEMS biosensor with unique functionalities, in terms of its ability to use antibody-antigen recognition, dielectrophoretic cell focusing, and impedance spectroscopy to achieve accurate low-level bacterial sensing capability. The dielectrophoretic manipulation of the cells enabled us to concentrate the bacterial cells inside the microchannel, which improved the overall performance of the device. The polyclonal anti-*E. coli* antibody coated sensing IDE array ensures specific sensing of *E. coli* 0157:H7 bacterial cells. The biosensor was able to successfully detect *E. coli* concentrations up to 39 CFU/ml within an overall time of 2 h.

ACKNOWLEDGMENTS

This project was supported in part by the National Science Foundation (Grant No. ECCS-0925612) and USDA-Capacity Building Grant.

[1]Center for Disease Control and Prevention, "Estimates of Foodborne Illness in the United States," 2014.
[2]Centers for Disease Control and Prevention, "Foodborne Outbreaks," 2015.
[3]Centers for Disease Control and Prevention, "CDC Current Outbreak List," 2015.
[4]R. L. Scharff, "Economic burden from health losses due to foodborne illness in the United States," J. Food Prot. **75**(1), 123–131 (2012).
[5]S. Park, R. W. Worobo, and R. A. Durst, "*Escherichia coli* O157:H7 as an emerging foodborne pathogen: A literature review," Crit. Rev. Food Sci. Nutr. **39**(6), 481–502 (1999).
[6]C. Murphy, C. Carroll, and K. N. Jordan, "Environmental survival mechanisms of the foodborne pathogen Campylobacter jejuni," J. Appl. Microbiol. **100**(4), 623–632 (2006).
[7]V. Velusamy, K. Arshak, O. Korostynska, K. Oliwa, and C. Adley, "An overview of foodborne pathogen detection: In the perspective of biosensors," Biotechnol. Adv. **28**(2), 232–254 (2010).
[8]M. Blanco *et al.*, "Serotypes, virulence genes, and intimin types of Shiga toxin (verotoxin)-producing *Escherichia coli* isolates from cattle in Spain and identification of a new intimin variant gene (eae-xi)," J. Clin. Microbiol. **42**(2), 645–651 (2004).
[9]P. Daly, T. Collier, and S. Doyle, "PCR-ELISA detection of *Escherichia coli* in milk," Lett. Appl. Microbiol. **34**(3), 222–226 (2002).
[10]A. Sen, T. Harvey, and J. Clausen, "A microsystem for extraction, capture and detection of *E. coli* O157:H7," Biomed. Microdevices **13**(4), 705–715 (2011).
[11]G. Papadakis *et al.*, "Micro-nano-bio acoustic system for the detection of foodborne pathogens in real samples," Biosens. Bioelectron. **111**, 52–58 (2018).
[12]J. Bhardwaj, S. Devarakonda, S. Kumar, and J. Jang, "Development of a paper-based electrochemical immunosensor using an antibody-single walled carbon nanotubes bio-conjugate modified electrode for label-free detection of foodborne pathogens," Sens. Actuators, B **253**, 115–123 (2017).
[13]A. Nehra, K. Pandey, K. P. Singh, S. Ahalawat, and R. P. Joshi, "Determination of *E. coli* by a graphene oxide-modified quartz crystal microbalance," Anal. Lett. **50**(12), 1897–1911 (2017).
[14]X. Liu, Y. Hu, S. Zheng, Y. Liu, Z. He, and F. Luo, "Surface plasmon resonance immunosensor for fast, highly sensitive, and *in situ* detection of the magnetic nanoparticles-enriched *Salmonella enteritidis*," Sens. Actuators, B **230**, 191–198 (2016).
[15]B. Thakur *et al.*, "Rapid detection of single *E. coli* bacteria using a graphene-based field-effect transistor device," Biosens. Bioelectron. **110**, 16–22 (2018).
[16]J.-Y. Hyeon and X. Deng, "Rapid detection of *Salmonella* in raw chicken breast using real-time PCR combined with immunomagnetic separation and whole genome amplification," Food Microbiol. **63**, 111–116 (2017).
[17]V. Escamilla-Gómez, S. Campuzano, M. Pedrero, and J. M. Pingarrón, "Gold screen-printed-based impedimetric immunobiosensors for direct and sensitive *Escherichia coli* quantisation," Biosens. Bioelectron. **24**(11), 3365–3371 (2009).
[18]H. Vaisocherová-Lísalová *et al.*, "Low-fouling surface plasmon resonance biosensor for multi-step detection of foodborne bacterial pathogens in complex food samples," Biosens. Bioelectron. **80**, 84–90 (2016).
[19]B. C. Towe and V. B. Pizziconi, "A microflow amperometric glucose biosensor," Biosens. Bioelectron. **12**(9–10), 893–899 (1997).
[20]C. Berggren, B. Bjarnason, and G. Johansson, "An immunological interleukine-6 capacitive biosensor using perturbation with a potentiostatic step," Biosens. Bioelectron. **13**(10), 1061–1068 (1998).
[21]M. Ciszkowska and Z. Stojek, "Voltammetry in solutions of low ionic strength. Electrochemical and analytical aspects," J. Electroanal. Chem. **466**(2), 129–143 (1999).
[22]C. Amatore, J. M. Savéant, and D. Tessier, "Charge transfer at partially blocked surfaces," J. Electroanal. Chem. Interfacial Electrochem. **147**(1–2), 39–51 (1983).
[23]K. Maruyama, H. Ohkawa, S. Ogawa, A. Ueda, O. Niwa, and K. Suzuki, "Fabrication and characterization of a nanometer-sized optical fiber electrode based on selective chemical etching for scanning electrochemical/optical microscopy," Anal. Chem. **78**(6), 1904–1912 (2006).

[24]Y.-S. Liu *et al.*, "Electrical detection of germination of viable model *Bacillus anthracis* spores in microfluidic biochips," Lab Chip **7**(5), 603–610 (2007).
[25]E. Nebling, T. Grunwald, J. Albers, P. Schäfer, and R. Hintsche, "Electrical detection of viral DNA using ultramicroelectrode arrays," Anal. Chem. **76**(3), 689–696 (2004).
[26]M. Barreiros dos Santos, J. P. Agusil, B. Prieto-Simón, C. Sporer, V. Teixeira, and J. Samitier, "Highly sensitive detection of pathogen *Escherichia coli* O157:H7 by electrochemical impedance spectroscopy," Biosens. Bioelectron. **45**, 174–180 (2013).
[27]S. G. Dastider, S. Barizuddin, M. Dweik, and M. F. Almasri "Impedance biosensor based on interdigitated electrode array for detection of *E. coli* O157: H7 in food products," Proc. SPIE **8369**, 83690Q (2012).
[28]M. Dweik, R. C. Stringer, S. G. Dastider, Y. Wu, M. Almasri, and S. Barizuddin, "Specific and targeted detection of viable *Escherichia coli* O157:H7 using a sensitive and reusable impedance biosensor with dose and time response studies," Talanta **94**, 84–89 (2012).
[29]S. G. Dastider, S. Barizuddin, Y. Wu, M. Dweik, and M. Almasri, "Impedance biosensor based on interdigitated electrode arrays for detection of low levels of *E. coli* O157:H7," in *2013 IEEE 26th International Conference on Micro Electro Mechanical Systems (MEMS)* (IEEE, 2013), pp. 955–958.
[30]S. G. Dastider, S. Barizuddin, M. Dweik, and M. Almasri, "A micromachined impedance biosensor for accurate and rapid detection of *E. coli* O157:H7," RSC Adv. **3**(48), 26297 (2013).
[31]S. Ghosh Dastider, S. Barizuddin, N. S. Yuksek, M. Dweik, and M. F. Almasri, "Efficient and rapid detection of *Salmonella* using microfluidic impedance based sensing," J. Sens. **2015**, 1–8.
[32]Y. Wang, Z. Ye, and Y. Ying, "New trends in impedimetric biosensors for the detection of foodborne pathogenic bacteria," Sensors **12**(12), 3449–3471 (2012).
[33]D. A. Boehm, P. A. Gottlieb, and S. Z. Hua, "On-chip microfluidic biosensor for bacterial detection and identification," Sens. Actuators, B **126**(2), 508–514 (2007).
[34]C. D. Chin and V. Linder, "Lab-on-a-chip devices for global health: Past studies and future opportunities," Lab Chip **7**(1), 41–57 (2007).
[35]D. Figeys and D. Pinto, "Lab-on-a-chip: A revolution in biological and medical sciences," Anal. Chem. **72**(9), 330A–335A (2000).
[36]H. A. Stone, A. D. Stroock, and A. Ajdari, "Engineering flows in small devices," Annu. Rev. Fluid. Mech. **36**(1), 381–411 (2004).
[37]B. H. Lapizco-Encinas, B. A. Simmons, E. B. Cummings, and Y. Fintschenko, "Dielectrophoretic concentration and separation of live and dead bacteria in an array of insulators," Anal. Chem. **76**(6), 1571–1579 (2004).
[38]P. R. C. Gascoyne, J. Noshari, T. J. Anderson, and F. F. Becker, "Isolation of rare cells from cell mixtures by dielectrophoresis," Electrophoresis **30**(8), 1388–1398 (2009).
[39]H.-S. Moon *et al.*, "Continuous separation of breast cancer cells from blood samples using multi-orifice flow fractionation (MOFF) and dielectrophoresis (DEP)," Lab Chip **11**(6), 1118 (2011).
[40]H. O. Fatoyinbo, M. C. McDonnell, and M. P. Hughes, "Dielectrophoretic sample preparation for environmental monitoring of microorganisms: Soil particle removal," Biomicrofluidics **8**(4), 044115 (2014).
[41]C. Choongho Yu, J. Vykoukal, D. M. Vykoukal, J. A. Schwartz, L. Li Shi, and P. R. C. Gascoyne, "A three-dimensional dielectrophoretic particle focusing channel for microcytometry applications," J. Microelectromech. Syst. **14**(3), 480–487 (2005).
[42]Y. Cao, P. C. Irwin, and K. Younsi, "The future of nanodielectrics in the electrical power industry," IEEE Trans. Dielectr. Electr. Insul. **11**(5), 797–807 (2004).
[43]See https://www.engineeringtoolbox.com/relative-permittivity-d_1660.html for "Relative permittivity—The dielectric constant" (accessed November 05 2018).
[44]D. Esteban-Ferrer, M. A. Edwards, L. Fumagalli, A. Juárez, and G. Gomila, "Electric polarization properties of single bacteria measured with electrostatic force microscopy," ACS Nano **8**(10), 9843–9849 (2014).